Pi2 onset time determination with information criterion

T. Higuchi
The Institute of Statistical Mathematics, Tokyo, Japan

S.-I. Ohtani
The Johns Hopkins University, Applied Physics Laboratory, Laurel, Maryland, USA

T. Uozumi and K. Yumoto
Department of Earth and Planetary Sciences, Kyushu University, Fukuoka, Japan

Received 22 May 2001; revised 18 July 2001; accepted 28 July 2001; published 16 July 2002.

[1] The present study proposes a new method to identify ground Pi2 onsets. The Pi2 wave is usually examined by applying a linear band-pass filter or something equivalent, such as wavelet convolution, to ground magnetometer data, and its onset is determined based on the amplitude of the extracted wave component. The proposed method is distinguished from such conventional methods in terms of the following points. First the proposed method does not filter or smooth data, rather it analyzes the original data. Second the proposed method determines the Pi2 onset so that the intervals before and after the onset can be optimally described by different time series models. The optimal partition is determined by minimizing the Akaike information criterion (AIC). The time series models adopted are general enough to apply to any nonstationary time series irrespective of its waveform, frequency, amplitude, and signal-to-noise ratio. As a result, the proposed procedure is free from the choice of a threshold and is therefore objective. The procedure is applied to simulation data, and it is confirmed that the procedure can determine the onset with the precision of the data's time resolution. An application to magnetic field data from 210° magnetic meridian (MM) stations suggests that our procedure can be used for examining the latitudinal and longitudinal dependence of the onset time. The proposed procedure is expected to be useful for examining issues that have been difficult to address with conventional methods because of the precision required for determining Pi2 onset. *INDEX TERMS:* 2752 Magnetospheric Physics: MHD waves and instabilities; 2788 Magnetospheric Physics: Storms and substorms; 2794 Magnetospheric Physics: Instruments and techniques; *KEYWORDS:* Pi2 onset time, AIC, switching model, ground magnetic stations

1. Introduction

[2] Pi2 pulsation is a damped oscillation with a period of 40–150 s (6.7–25 mHz) (see a recent review article by *Olson* [1999]). The excitation of the Pi2 wave is closely related to the substorm trigger [*Saito et al.*, 1976] and therefore Pi2 onset is often used for identifying substorm onsets. Pi2 pulsation is observed in a wide latitudinal range, from the magnetic equator to the polar cap, although the characteristics of the Pi2 pulsation may differ depending on the latitude [*CPMN Group*, 2001]. Pi2 pulsation can also be observed in a much wider longitudinal range than the initial auroral brightening or the negative bay onset. Thus, in contrast to other onset identifiers, the limited distribution of ground stations is less serious for the detection of Pi2 pulsations.

[3] Substorm onset timing is a key issue for understanding the substorm trigger mechanism, and several studies have been devoted to this issue recently [e.g., *Ohtani et al.*, 1999; *Liou et al.*, 2000]. The onset of Pi2 pulsation provides a proxy of substorm onset, which was originally defined based on the auroral image, and sometimes the Pi2 onset is (implicitly) assumed to coincide with auroral breakup. Such an assumption needs to be observationally tested, especially because determination of the onset is crucial for investigating tail substorm dynamics. The fast plasma flow in the plasma sheet, which is often regarded as an effect of near-Earth neutral reconnection, is occasionally observed in the midtail region prior to Pi2 onsets [e.g., *Shiokawa et al.*, 1998; *Nagai et al.*, 1998], whereas in some events, magnetic fluctuations associated with tail current disruption are observed in the near-Earth region prior to Pi2 onsets [e.g., *Ohtani et al.*, 1998]. The delay that these studies concern is 5 min at maximum and is generally shorter. [e.g., *Sergeev et al.*, 1995; *Shiokawa et al.*, 1998; *Nagai et al.*, 1998; *Ohtani et al.*, 1999]. The situation is even more complex because the timing of the Pi2 onset relative to the corresponding auroral breakup is controversial [*Liou et al.*, 2000]. However, the Pi2 onset is often identified by visual inspection, and therefore its determination tends to be subjective or ad hoc. Furthermore, the delay concerned is close to the period of the Pi2 pulsation. Thus the Pi2 onset needs to be determined

0148-0227/02/2001JA003505$09.00

with precision much shorter than the wave period. Another relevant issue is the time difference of Pi2 onsets at different stations, that is, the (apparent) propagation of Pi2 waves in latitude and longitude on the ground. Precision required for examining such propagation is also much shorter than the typical period of the Pi2 pulsation.

[4] Development of a procedure to determine Pi2 onset automatically and accurately would be desirable. Automatic determination of Pi2 onset has been carried out by employing various data adaptive filters such as wavelet analysis [*Nose' et al.*, 1998; *Tsunezawa et al.*, 1999] and an artificial neural network (ANN) [*Sutcliffe*, 1997]. Although these methods are useful for selecting Pi2 onsets, the precision of the determined onset time does not meet our requirement, for example.

[5] When the background magnetic field and/or the amplitude of noisy component change around the initial period of Pi2 pulsations, any linear band-pass filter generates a pseudo precursor prior to a true onset time. The previous methods use the wave amplitude or something equivalent for selecting onsets, which is defined by applying a wavelet convolution procedure or an appropriate smoothing method [*Takahashi et al.*, 1995; *Nose' et al.*, 1998; *Tsunezawa et al.*, 1999; *Liou et al.*, 2000; *Uozumi et al.*, 2000; *Kepko and McPherron*, 2001]. Therefore those methods inevitably disregard information about wave components with frequencies higher than the Pi2 frequency. In addition, the threshold for selecting the Pi2 pulsation tends to be arbitrary, which affects the estimated onset time. The approach using an ANN mitigates this problem of a reasonable choice of thresholds but still suffers from insufficient resolution in estimating the onset time because the lower-frequency components of the amplitude spectrum are used as input data in the ANN [*Sutcliffe*, 1997].

[6] The present paper reports an objective procedure we developed to determine the onset time of the Pi2 pulsation. We applied this procedure to magnetic field data from the 210° magnetic meridian (MM) observation [*Yumoto et al.*, 1996]. Section 2 explains the switching model approach. Section 3 describes a procedure to determine a Pi2 onset time. In section 4 we demonstrate the procedure by applying it to a simulation data set. In section 5 we apply the procedure to ground data acquired from the 210° MM observation network. In section 6 we discuss the analysis result in terms of a precision. Section 7 gives a brief summary.

2. Model Switching Approach

2.1. Time Series Models

[7] Three time series models are adopted in this study to describe sequential data H_n in the time domain: Model m, where m = 1, 2, 3. Model 1 assumes that the time series contains no periodic variation associated with the Pi2 pulsation. This model consists of a smooth variation of the background magnetic field and high-frequency/irregular fluctuations, which correspond to noises or unknown physical processes. A decomposition approach similar to Model 1 for extraction of the Pi2 pulsation was proposed by *Itonaga and Kitamura* [1994]. Model 2 is for describing monochromatic pseudocyclical variations such as Pi2 pulsations superposed on a smooth change of the background magnetic field. Model 3 describes more complicated signatures whose power spectrum contains a line and is continuous elsewhere.

[8] These three time series models can be expressed as follows:

$$\text{Model 1}: \quad H_n = t_n^{(1)} + w_n^{(1)}$$

$$\text{Model 2}: \quad H_n = t_n^{(2)} + q_n^{(2)} + w_n^{(2)}$$

$$\text{Model 3}: \quad H_n = t_n^{(3)} + q_n^{(3)} + r_n + w_n^{(3)}$$

where $w_n^{(m)}$ (m = 1, 2, 3) is the observation noise, which follows a Gaussian distribution with zero mean and unknown variance of $\sigma^{2,(m)}$: $w_n^{(m)} \sim N(0, \sigma^{2,(m)})$. $t_n^{(m)}$ is a stochastic trend component and follows a system model [*Kitagawa*, 1981; *Higuchi*, 1991; *Kitagawa and Gersch*, 1996]

$$t_n^{(m)} = 2t_{n-1}^{(m)} - t_{n-2}^{(m)} + v_n^{t,(m)}, \quad v_n^{t,(m)} \sim N\left(0, \tau_t^{2,(m)}\right), \tag{1}$$

where $v_n^{t,(m)}$ is the system noise which follows a Gaussian distribution with zero mean and unknown variance of $\tau_t^{2,(m)}$. A ratio of $\tau_t^{2,(m)}$ to $\sigma^{2,(m)}$ controls the smoothness of the trend component: see *Kitagawa and Gersch* [1996, Section 8] for the performance of this trend model.

[9] The $q_n^{(m)}$ (m = 2, 3) describes a quasi-periodic oscillation (QPO), which is represented by the following second-order stochastic difference equation:

$$q_n^{(m)} = 2\cos\left(2\pi f_c^{(m)}\Delta t\right) q_{n-1}^{(m)} - q_{n-2}^{(m)} + v_n^{q,(m)}, \quad v_n^{q,(m)} \sim N\left(0, \tau_q^{2,(m)}\right), \tag{2}$$

where $f_c^{(m)}$ corresponds to the frequency of the Pi2 pulsation, which in our procedure is treated as an unknown parameter that does not have to be given beforehand. Here Δt is a sampling interval. For an extreme case of $\tau_q^{2,(m)} = 0$, $q_n^{(m)}$ is reduced to either a purely sinusoidal signal or zero. The system noise in (2) makes the cycle stochastic rather than deterministic, and accordingly, the QPO model describes a periodic component of distinct frequency $f_c^{(m)}$ with stochastically time-varying amplitude and phase [*Higuchi et al.*, 1988]. Thus the QPO model is suitable for mathematically representing Pi2 pulsations.

[10] We add a locally stationary component r_n to Model 3, which is represented by an auto-regressive (AR) model as

$$r_n = \sum_{l=1}^{L_{AR}} a_l r_{n-l} + v_n^r, \quad v_n^r \sim N\left(0, \tau_r^2\right). \tag{3}$$

In this study we set L_{AR} = 4. The performance of an AR model for various applications is given by *Akaike and Kitagawa* [1998].

2.2. State Space Representation

[11] The time series models mentioned above can be expressed by the state space model (SSM) [*Anderson and Moore*, 1979; *Kitagawa*, 1981; *Higuchi*, 1991]

$$\begin{cases} H_n = D^{(m)}\mathbf{x}_n^{(m)} + w_n^{(m)} \\ \mathbf{x}_n^{(m)} = F^{(m)}\mathbf{x}_{n-1}^{(m)} + G^{(m)}\mathbf{v}_n^{(m)}. \end{cases} \tag{4}$$

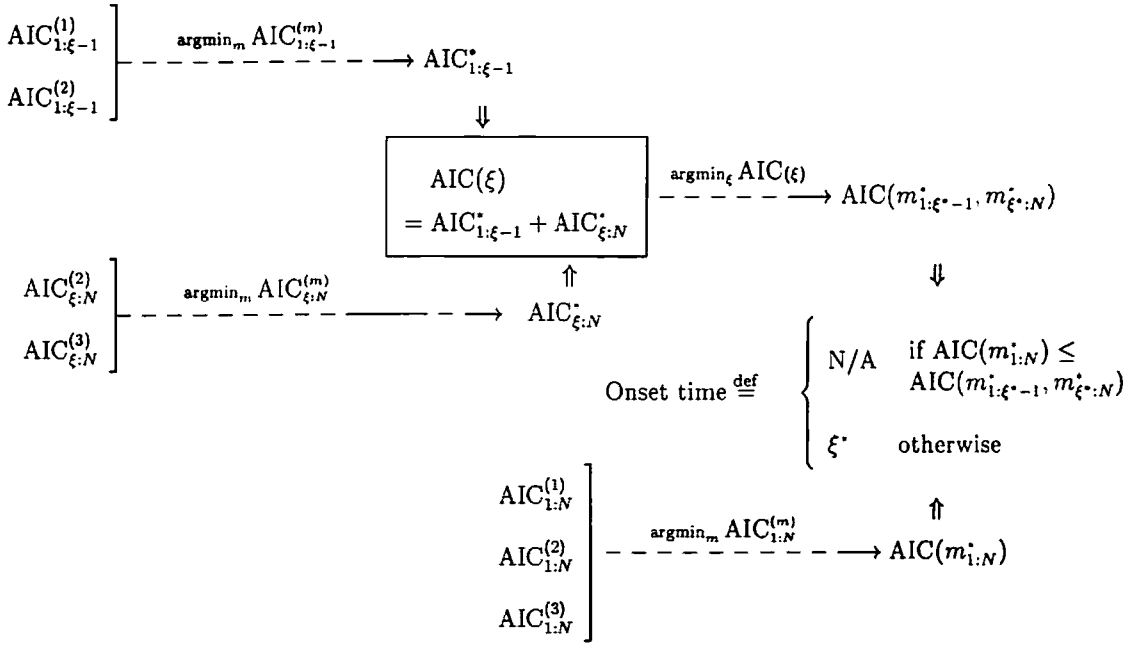

Figure 1. Schematic illustration of a whole procedure for an onset time determination.

One merit of using this SSM is that we can employ computationally efficient recursive calculation algorithms. called the Kalman filter and smoother, for estimating state variables such as $t_n^{(m)}$, $q_n^{(m)}$, and r_n.

[12] As an example, we show only the SSM for Model 3, which is the most complicated of the three models. The SSM for Model 3 consists of the following vectors and matrices:

$$\mathbf{x}_n^{(3)} = \left[t_n^{(3)}, t_{n-1}^{(3)}, q_n^{(3)}, q_{n-1}^{(3)}, r_n, r_{n-1}, r_{n-2}, r_{n-3}\right]'$$

$$D^{(3)} = [1,\ 0,\ 1,\ 0,\ 1,\ 0,\ 0,\ 0],$$

$$F^{(3)} = \begin{pmatrix} 2 & -1 & & & & & & \\ 1 & & & & & & & \\ & & C & -1 & & & & \\ & & 1 & & & & & \\ & & & & a_1 & a_2 & a_3 & a_4 \\ & & & & 1 & & & \\ & & & & & 1 & & \\ & & & & & & 1 & \end{pmatrix},$$

$$G^{(3)} = \begin{pmatrix} 1 & & & \\ 0 & & & \\ & 1 & & \\ & 0 & & \\ & & 1 & \\ & & 0 & \\ & & 0 & \\ & & 0 & \end{pmatrix}, \quad \mathbf{v}_n^{(3)} = \begin{bmatrix} v_n^{t,(3)} \\ v_n^{q,(3)} \\ v_n^{r} \end{bmatrix}$$

where $C = 2\cos(2\pi f_c^{(3)}\Delta t)$. The prime denotes transposition, and the empty entries of $F^{(3)}$ and $G^{(3)}$ are all zero. Here $\mathbf{v}_n^{(3)} \sim N(0, R^{(3)})$ with a diagonal variance matrix of $R^{(3)} = \text{diag}(\tau_t^{2,(3)}, \tau_q^{2,(3)}, \tau_r^2)$. Here $\tau_t^{2,(3)}$, $\tau_q^{2,(3)}$, and τ_r^2 are unknown parameters to be optimized. Thus Model 3 includes nine unknown parameters:

$$\theta^{(3)} = \left[\sigma^{2,(3)}, \tau_t^{2,(3)}, f_c^{(3)}, \tau_q^{2,(3)}, \tau_r^2, a_1, a_2, a_3, a_4\right]'. \quad (5)$$

The SSMs for Model 1 and Model 2 are easily defined by reducing the dimensions of the vectors and matrices.

2.3. Parameter Estimation and AIC

[13] When we apply Model-m to a data set $H_{n_1:n_2} = [H_{n_1}, H_{n_1+1}, \ldots, H_{n_2-1}, H_{n_2}]$, the Kalman filter and smoother algorithms for the given parameter $\theta^{(m)}$ provide an estimate of the state vector. $\hat{\mathbf{x}}_n^{(m)}$ [*Kitagawa*, 1981; *Higuchi*, 1991]. The procedure for obtaining $\hat{\mathbf{x}}_n^{(m)}$ is described in appendix 1. The unknown parameter vector $\theta^{(m)}$ can be determined by maximizing the log-likelihood for $H_{n_1:n_2}$

$$\ell\left(H_{n_1:n_2}|\theta^{(m)}\right) = \sum_{n=n_1}^{n_2} \log p\left(H_n|H_{n_1:n-1}, \theta^{(m)}\right), \quad (6)$$

where $p\left(H_n|H_{n_1:n-1}, \theta^{(m)}\right)$, is the likelihood of H_n given $H_{n_1:n-1}$ and is obtained as a by-product in the filtering step of the Kalman filter (see appendix 1). The optimal $\theta^{(m)}$ is denoted as $\theta^{(m)*}$. The final estimate of the state vector, $\mathbf{x}_n^{(m)*}$, is obtained by applying the Kalman filter and smoother algorithms to the SSM with $\theta^{(m)*}$.

[14] The fitness of Model m can be evaluated by the Akaike information criterion (AIC) [*Akaike*, 1974; *Sakamoto et al.*, 1986]. The value of AIC for Model m, which is applied to data $H_{n_1:n-1}$, $\left(\text{AIC}_{n_1:n_2}^{(m)}\right)$ is defined as follows [*Kitagawa*, 1981]:

$$\text{AIC}_{n_1:n_2}^{(m)} = -2\ell\left(H_{n_1:n_2}|\theta^{(m)\bullet}\right) + 2\left[\dim\left(\theta^{(m)}\right) + \dim\left(\mathbf{x}_{n_1-1}^{(m)}\right)\right]. \quad (7)$$

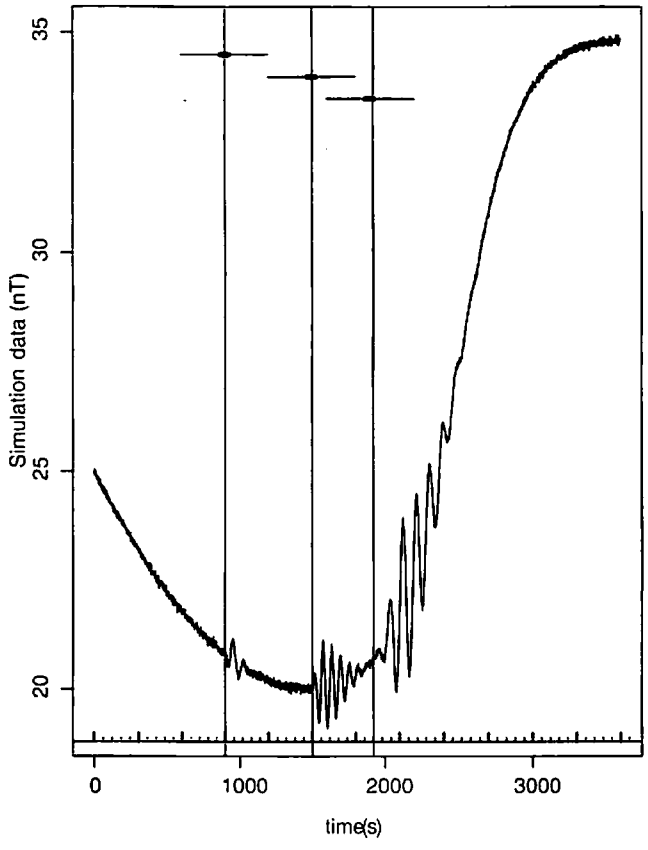

Figure 2. Simulation data. The three thin horizontal bars at the top indicate the data windows adopted for an onset time determination of each wave packet. The thick part of each bar represents the interval for which an optimal ξ is searched within each data window. The three vertical lines indicate the given true onset times: $\xi_{[1]}^{\text{true}} = 901$ s, $\xi_{[2]}^{\text{true}} = 1501$ s, and $\xi_{[3]}^{\text{true}} = 1921$ s.

A model with smaller $\text{AIC}_{n_1:n_2}^{(m)}$ is regarded as a better model.

3. Determination of Onset Time

3.1. Division of Data Set

[15] Suppose that a wave packet of a Pi2 pulsation starts at time ξ within an interval of total data points N, which we call the data window henceforth. Hence the entire data set $H_{1:N}$ is divided into two subintervals:

$$H_{1:N} = [\overbrace{H_1, \ldots, H_{\xi-1}}^{H_{1:\xi-1}} | \overbrace{H_\xi, \ldots, H_N}^{H_{\xi:N}}]. \quad (8)$$

Obviously, Model 2 and Model 3 are candidates for describing $H_{\xi:N}$. The better model is determined by comparing $\text{AIC}_{\xi:N}^{(2)}$ and $\text{AIC}_{\xi:N}^{(3)}$, and is denoted by $m_{\xi:N}^*$. For simplicity, $\text{AIC}_{\xi:N}^{(m_{\xi:N}^*)}$ is designated by $\text{AIC}_{\xi:N}^*$ hence-forth.

[16] No Pi2 pulsation is usually expected for an interval before ξ, and therefore Model 1 is first considered as an appropriate time series model for $H_{1:\xi-1}$. However, if the interval includes a Pi2 pulsation with different wave characteristics from those of the Pi2 pulsation during $H_{\xi:N}$, Model 2 could be applied to $H_{1:\xi-1}$. For example, it is possible for the two different Pi2 pulsations to be observed successively in a data window. A choice of the time series model can be made by comparing two values of AIC: $\text{AIC}_{1:\xi-1}^{(1)}$ and $\text{AIC}_{1:\xi-1}^{(2)}$. A chosen model is specified by $m_{1:\xi-1}^*$.

[17] The best partition of the data window, namely an optimal ξ, can be obtained by evaluating for $H_{1:N}$, which is denoted by $\text{AIC}(m_{1:\xi-1}^*, m_{\xi:N}^*)$ in this study and is given by [*Takanami*, 1998]

$$\text{AIC}(m_{1:\xi-1}^*, m_{\xi:N}^*) = \text{AIC}_{1:\xi-1}^* + \text{AIC}_{\xi:N}^*. \quad (9)$$

Here $\text{AIC}(m_{1:\xi-1}^*, m_{\xi:N}^*)$ is a function of ξ: $\text{AIC}(m_{1:\xi-1}^*, m_{2\xi:N}^*) = \text{AIC}(\xi)$. An optimal ξ, denoted by ξ^*, is determined by searching ξ which minimizes $\text{AIC}(m_{1:\xi-1}^*, m_{\xi:N}^*)$ between an interval centered at $N/2$ ($N/2 - L \le \xi \le N/2 + L$).

3.2. Onset Time Definition

[18] The procedure described in section 3.1 assumes that there is a Pi2 onset in the given data window $H_{1:N}$, which can be determined by optimally fitting different models to intervals before and after the onset. However, we need to consider two cases in which the data division is unnecessary. One is that the interval does not include any signature associated with a Pi2 pulsation. In such a case, Model 1 must be applied to $H_{1:N}$. The fitness is evaluated by $\text{AIC}_{1:N}^{(1)}$. The other case is that a Pi2 pulsation is dominant throughout the the interval without changing its characteristics. In this case, Model 2 or Model 3 can be regarded as an appropriate time series model for $H_{1:N}$, and the model's fitness can be evaluated based on $\text{AIC}_{1:N}^{(2)}$ and $\text{AIC}_{1:N}^{(3)}$. The model with the minimum value among $\text{AIC}_{1:N}^{(2)}$, $\text{AIC}_{1:N}^{(2)}$, and $\text{AIC}_{1:N}^{(3)}$ is chosen as the best single-model fit to $H_{1:N}$ and is denoted by $m_{1:N}^*$. The AIC value with $m_{1:N}^*$ is represented by $\text{AIC}(m_{1:N}^*)$.

[19] The final step of the onset time determination is to compare two AIC values: $\text{AIC}(m_{1:N}^*)$ and $\text{AIC}(m_{1:\xi^*-1}^*, m_{\xi^*:N}^*)$. If $\text{AIC}(m_{1:\xi^*-1}^*, m_{\xi^*:N}^*)$ is smaller than $\text{AIC}(m_{1:N}^*)$, ξ^* is identified as an onset time. Otherwise no onset time is identified: ξ = N/A for $\text{AIC}(m_{1:N}^*) \le \text{AIC}(m_{1:\xi^*-1}^*, m_{\xi^*:N}^*)$. The whole procedure is schematically illustrated in Figure 1. It should be remarked that our procedure has a resolution identical to the sampling time from the viewpoint of the algorithm.

3.3. Additional Criteria

[20] In practice we impose several additional criteria for model evaluation beyond the minimization of AIC. When wave activity for the first wave cycle after the onset time is insignificantly small, for example, less than the standard deviation of the estimated observation noise sequences, $\hat{\sigma}^{(m)}$ (see Appendix), such decomposition is meaningless. If the mean amplitude of the QPO component for the first quarter wave cycle is smaller than $3\hat{\sigma}^{(m)}$, the procedure discriminates such a case by giving an extremely larger value to $\text{AIC}_{\xi:N}^{(m)}$ ($m = 2$ or 3). Here it should be noted that $\hat{\sigma}^{(m)}$ is not given empirically but is determined by the procedure in the course of maximizing the log-likelihood. That is, it is data-

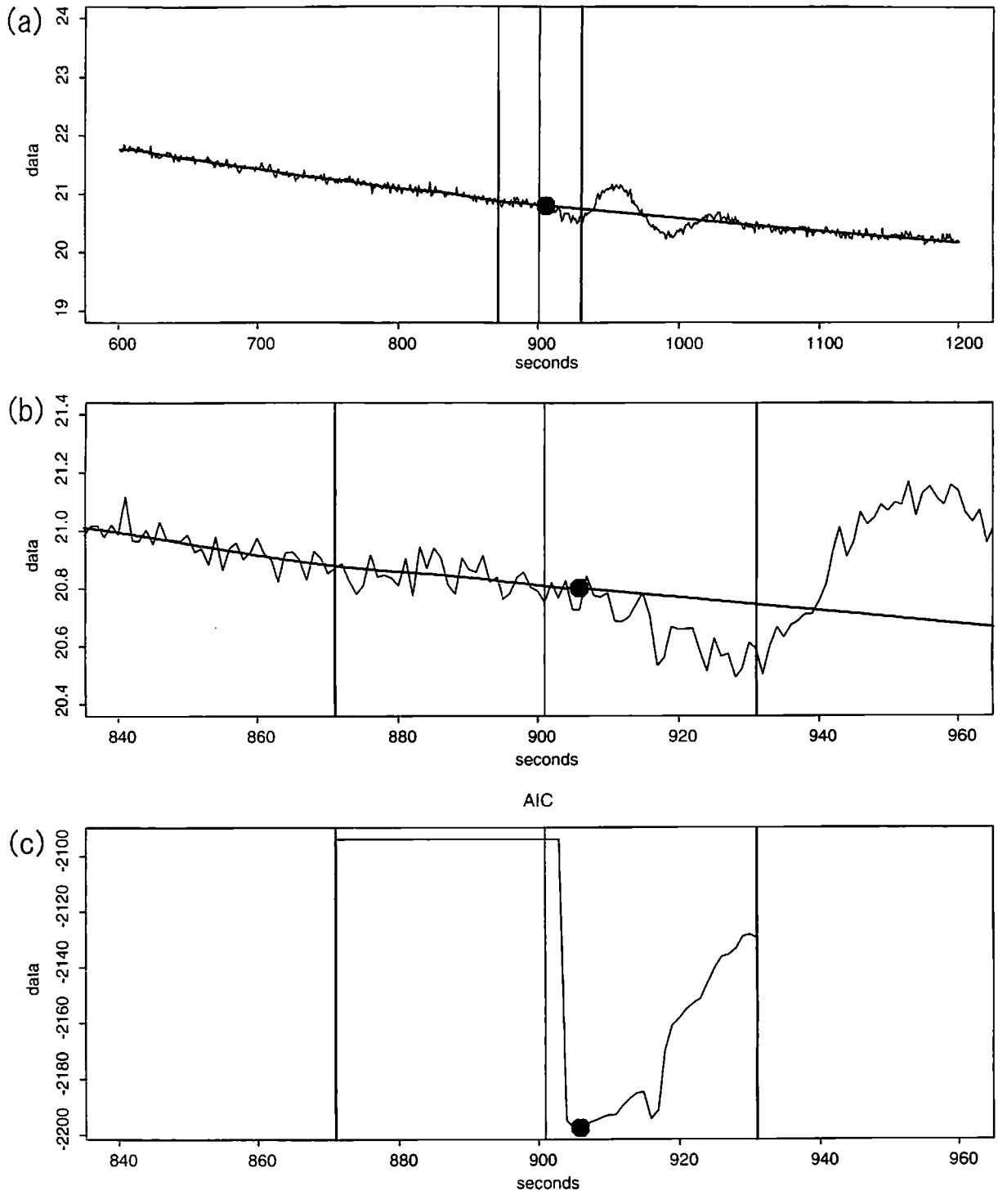

Figure 3. Result for the first packet. (a) Simulation data and estimated trend. The thin vertical line indicate the given true onset time $\xi_{[1]}^{true}$. The two thick vertical lines represent an interval for which the optimal onset time $\xi_{[1]}^{*}$ is searched. (b) Enlarged version of Figure 3a. (c) AIC values as a function of ξ. AIC($m_{1:\xi-1}^{*}$, $m_{\xi:N}^{*}$). (Note the circles indicate the optimal ξ, $\xi_{[1]}^{*}$.)

adaptive, and therefore it does not depend on the signal-to-noise ratio. It is again important to understand that $\tilde{\sigma}^{(m)}$ need not be specified beforehand. This is an important difference from previous approaches such as [*Kepko and McPherron*, 2001], who adopted as σ the standard deviation of data during 30 min prior to Pi2 onsets. Another added criterion is that if $\hat{\sigma}^{(m)}$ is smaller than a data resolution such as 0.01 nT, such decomposition is owing to the overfitting of a time series model to the data. We also assign an outlier to AIC for this case.

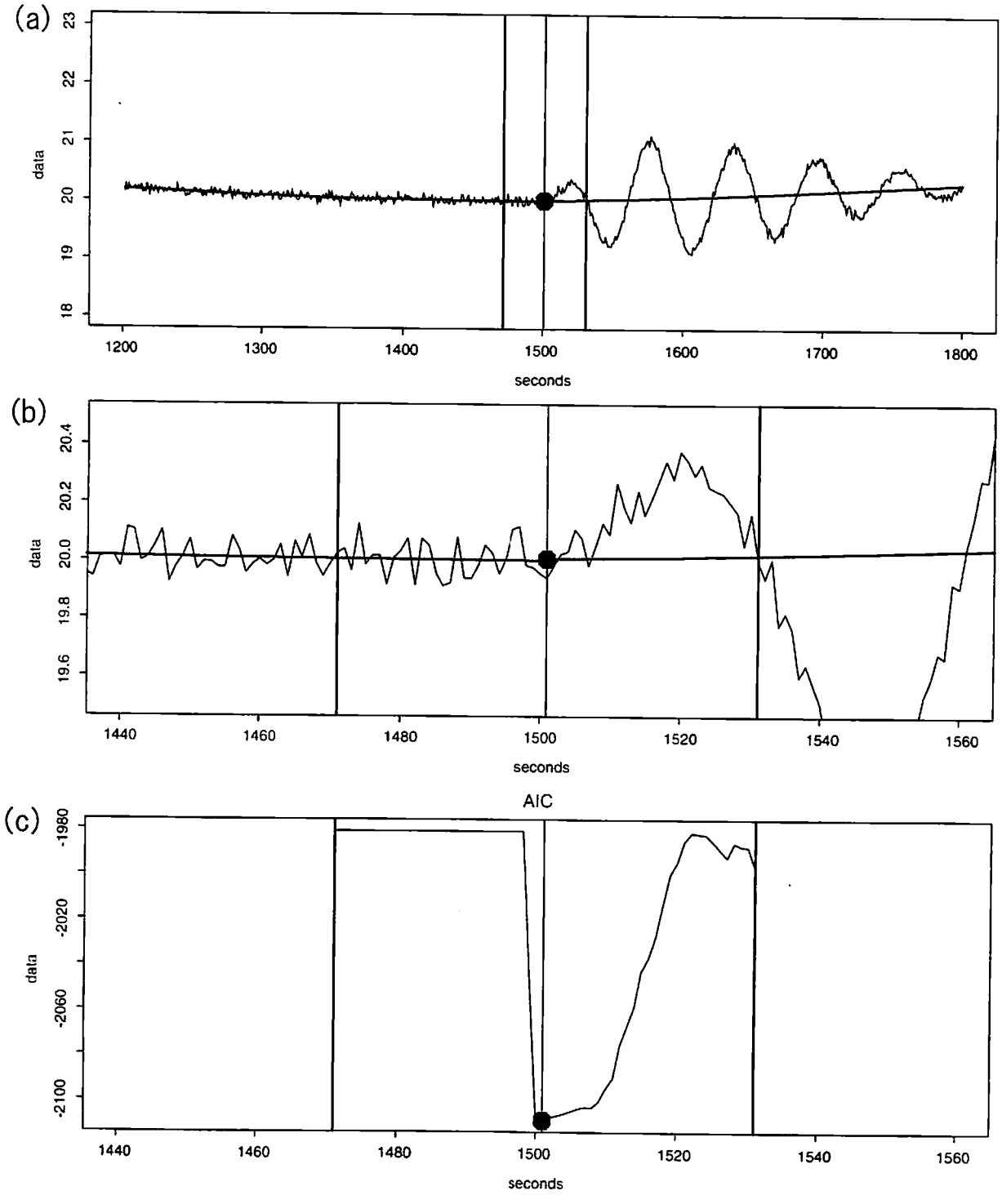

Figure 4. Result for the second packet.

[21] Since our model does not impose any constraint on the phase information, a QPO component extracted by our procedure starts with either an increase or a decrease. However, we found in our application (section 5) that an identified onset occasionally jumps by the half wave period from onsets identified for nearby stations, making it difficult to systematically understand the spatial (latitudinal) variation of onset times. Thus we decided to impose an additional restriction that the H component of the Pi2 pulsation starts with a positive change, which is realized by assigning an outlier to AIC if the first quarter wave cycle after a determined Pi2 onset is negative. This restriction should be reasonable since the Pi2 wave is believed to be generated by plasma compression in association with the substorm trigger. Note that we usually use Pi2 onsets detected in the midnight sector for identifying substorm onsets. However,

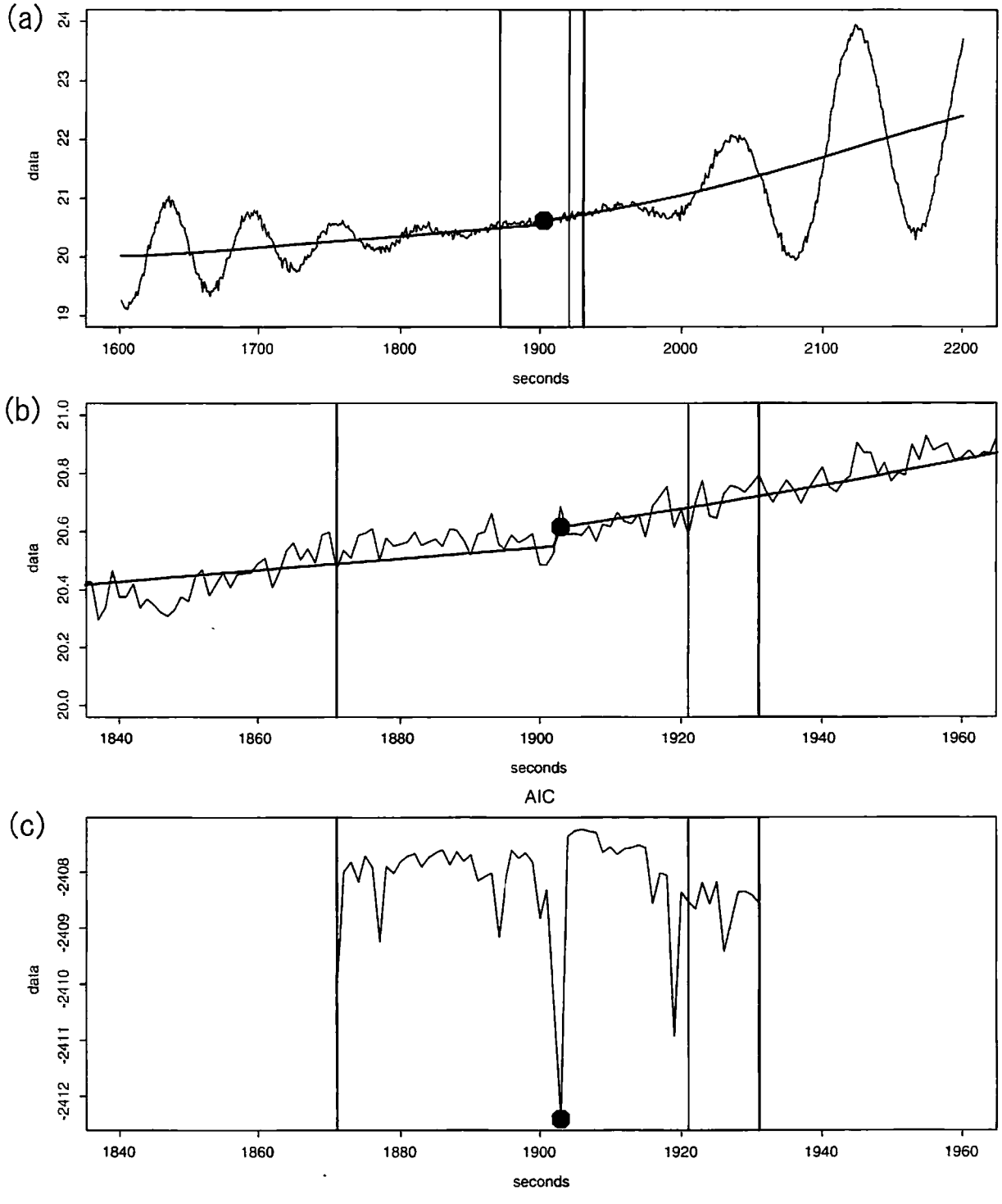

Figure 5. Result for the third packet.

some caution needs to be exercised when applying our procedure to Pi2 onsets detected at the flanks.

4. Simulation Data Analysis

[22] We tested our procedure with simulation data, which we created based on a midlatitude Pi2 event that *Liou et al.* [2000, 2001] and *Kepko and McPherron* [2001] debated in terms of the onset timing. The resolution of the data is 1 s, and the entire data set consists of 3600 points. The simulation data set, which is plotted in Figure 2, includes three packets of Pi2 pulsations. Their onset times are $\xi_{[1]}^{true} = 901$ s, $\xi_{[2]}^{true} = 1501$ s, and $\xi_{[3]}^{true} = 1921$ s, where [1], [2], and [3] indicate the first, second, and third wave packet in the simulation data. The wave periods are 75, 60, and 90 s, respectively. The maximum wave amplitudes are 0.5, 1, and 2 nT. Whereas the first wave packet is designed to start with a decrease, the second and third wave packets begin with an

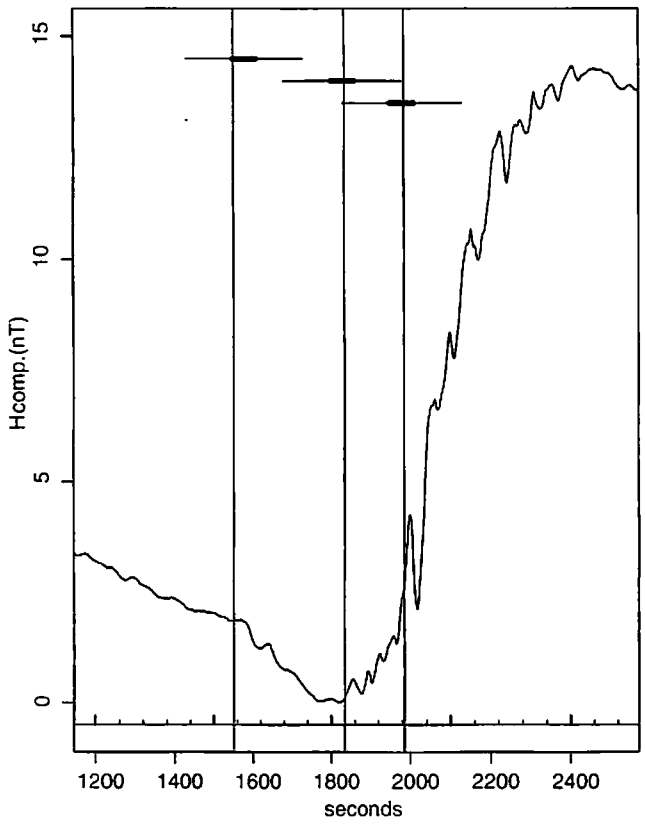

Figure 6. The raw H component data observed at KAK on March 1, 1997. The three vertical lines indicate the estimated onset times for each packet: $\xi^*_{[1]}$, $\xi^*_{[2]}$, and $\xi^*_{[3]}$. The three horizontal bars represent the data window for each packet. The thick parts of each bar represent the interval for which an optimal ξ is searched.

increase. The noise sequence is generated by drawing from a Gaussian distribution with zero mean and a standard deviation of 0.05; its ratio to the minimum amplitude among the three packets is 10%. The objective of this simulation study is to check the ability of our procedure to capture a wave signature irrespective of the sign of the initial variation, that is, whether it starts with an increase or a decrease. We did not require that the wave component starts with an increase, although when applying the procedure to actual data in section 5, we did require the increase.

[23] Although we frequently observe multiple-onset Pi2 pulsations, our procedure is designed to determine one onset within a data window. Thus a smaller data window size N is preferable in terms of the algorithm of the procedure. However, a smaller data window is unfavorable in terms of the model selection because the AIC value is less stable for a smaller number of data points, which makes the model selection less reliable. Since there is no theoretical framework for this trade-off problem, we adopted an empirical approach based on several simulation studies. We set $N_{\text{simu}} = 600$ in this study. An interval over which a search for an optimal ξ is performed is defined by $N/2 - L \le \xi \le N/2 + L$ in section 3.1. In this study we set $L = 30$. Then $\text{AIC}(m^*_{1:\xi-1}, m^*_{\xi:N})$ is calculated as a function of ξ between 270 and 330 s for each data window.

[24] Figure 3 shows the result of applying our procedure to the first Pi2 packet. Figure 3a plots only data points within this data window, on which a trend curve estimated by the procedure is superposed. The thin vertical line marks the given true onset time. The two thick vertical lines indicate an interval for searching ξ^*. The circle marks an estimated onset time, $\xi^*_{[1]} = 906$ s. Figure 3b shows a close-up of Figure 3a. Figure 3c plots $\text{AIC}(m^*_{1:\xi-1}, m^*_{\xi:N})$ for the same time interval as Figure 3b. As mentioned above, $\text{AIC}(m^*_{1:\xi-1}, m^*_{\xi:N})$ is calculated for the interval bounded by two thick vertical lines. The ξ^* is defined by ξ with the minimum AIC. The constant and large value of AIC before $t = 904$ s is actually truncated from the value we set as an outlier for not satisfying the additional criteria mentioned in section 3. The selected models are $m^*_{1:\xi^*-1} = 1$ and $m^*_{\xi^*:N} = 2$ before and after the onset, respectively, confirming the absence of the Pi2 pulsation before $n = \xi^*$. The estimation error, namely, a discrepancy of ξ^* from the true value given by $\xi^*_{[1]} - \xi^{\text{true}}_{[1]}$ is only 5 s. A visual inspection to Figure 3b suggests that our procedure is capable of identifying an onset time with high precision.

[25] Figures 4 and 5 show the results for the second and third packets, respectively, in the same format as Figure 3. For the second packet, ξ^*_2 is identical to the true onset time. For the third packet, the determination of the onset time is more difficult. As shown in Figure 5b, the residual effect of the second packet is included in the window, although its amplitude continues to decrease and reaches

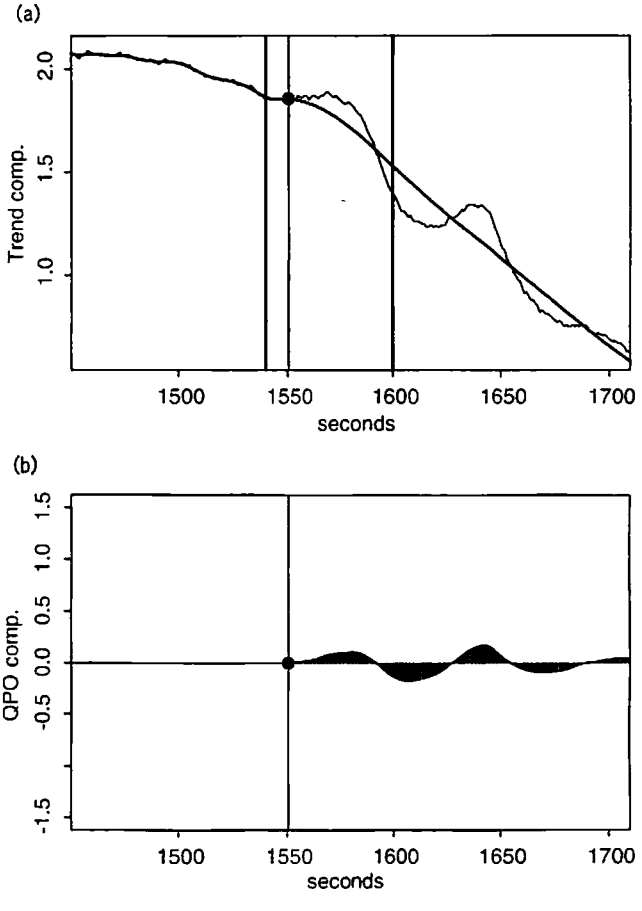

Figure 7. Result for the first wave packet at KAK.

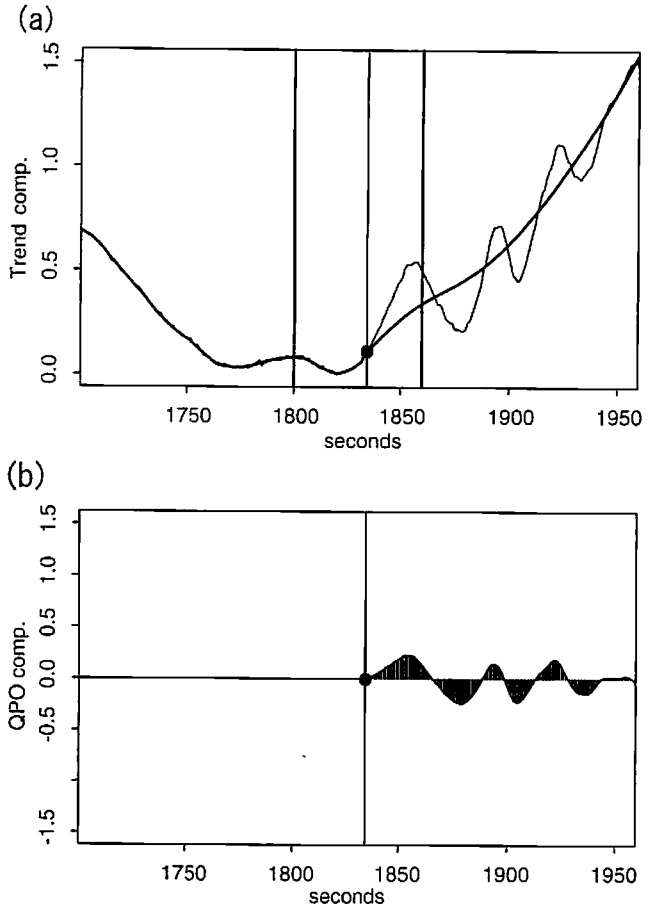

Figure 8. Result for the second wave packet at KAK.

the observation noise level around the onset time of the third packet. The estimated onset time is $\xi^*_{[3]} = 1903$ s. The difference from the true value, $\xi^*_{[3]} - \xi^{true}_{[3]} = 18$ s, is larger than the differences for the first and second packets. However, the ratio of the estimation error to the wave period of the third packet is only 20%. We therefore infer that the procedure can determine the onset time with precision better than visual inspection even for such a complicated situation. It should be noted that AIC($m^*_{1:\xi-1}$, $m^*_{\xi:N}$) takes the second minimum value at 1919 s, which is only 2 s off the true onset time. Thus, by taking into account of ξ with local minima, we can enumerate candidates for possible onset times with a probabilistic reliability. The selected models are $m^*_{1:\xi^*-1} = 2$ and $m^*_{\xi^*:N} = 2$ before and after the onset, respectively, indicating that the procedure successfully identified two distinct Pi2 waves.

5. Application

[26] Figure 6 shows the H magnetic field component measured at Kakioka (KAK) in Japan on March 1, 1997. The time resolution of data is 1 s. The horizontal axis represents seconds from 1300:00 UT. This event includes multiple onsets and was closely examined by *Liou et al.* [2000, 2001] and *Kepko and McPherron* [2001] in terms of the onset determination. A visual inspection of Figure 6 suggests that there are three Pi2 pulsation packets starting around 1326 UT (1560 s), 1330 UT (1850 s), and 1332 UT (1920 s). The Pi2 pulsations of the second- and third-wave packets were examined in detail previously in terms of a sophisticated approach to the onset time determination rather than a visual inspection [*Kepko and McPherron*, 2001]. Three horizontal bars shown in the top indicate the data windows adopted to determine an onset time for each wave packet. We set $N_{case} = 300$ for this case study because of the wave's shorter periods than those in the simulation study ($N_{simu} = 600$). The thick part for each bar represents the interval for which an optimal ξ is searched within each data window. Three vertical lines indicate the estimated onset times for each wave packet: $\xi^*_{[1]} = 1325{:}51$ (1551 s), $\xi^*_{[2]} = 1330{:}35$ (1835 s), and $\xi^*_{[3]} = 1333{:}05$ (1985 s).

[27] Figure 7 shows the result for the first wave packet at KAK. Figure 7a plots raw data and the estimated trend component for the interval around the optimal $\xi_{[1]}$. Two thick vertical lines indicate the searched interval. The thin line marks $\xi^*_{[1]}$. Figure 7b demonstrates the QPO component corresponding to the Pi2 pulsation. The vertical line marks $\xi^*_{[1]}$. The selected models are $m^*_{1:\xi^*-1} = 1$ and $m^*_{\xi^*:N} = 2$ before and after the onset, respectively. Figure 8 shows the result for the second wave packet in the same format as Figure 7. This onset was selected as the first onset by *Kepko and McPherron* [2001]. The selected models are $m^*_{1:\xi^*-1} = 1$ and $m^*_{\xi^*:N} = 2$. Figure 9 shows the result for the third wave packet, which *Liou et al.* [2000] selected as

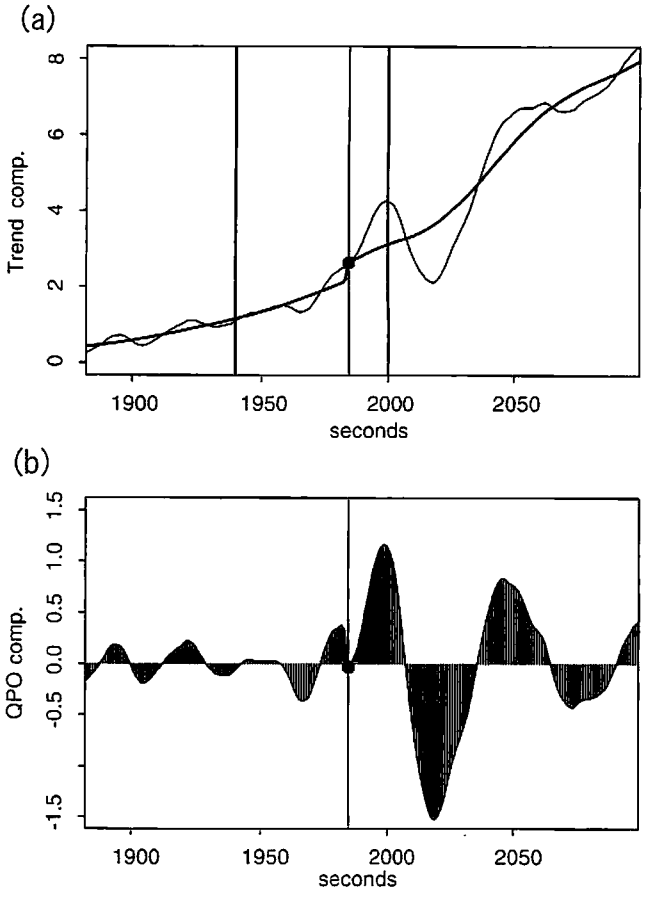

Figure 9. Result for the third wave packet at KAK.

Table 1. Coordinates of Stations

Station Name	Abbrev.	GG lat.	GG lon.	GM lat.	GM lon.	L	$\xi^*_{[1]}$ ([s])	$\xi^*_{[2]}$	$\xi^*_{[3]}$
Magadan	MGD	59.97	150.86	53.49	218.75	2.87	1551	1838	1984
Popov Island	PPI	42.98	131.73	36.27	203.74	1.56	1545	1826	1986
Kakioka	KAK	36.23	140.18	26.94	208.29	1.26	1551	1835	1985
Kagoshima	KAG	31.48	130.72	24.37	202.36	1.22	1556	1829	1985
Muntinlupa	MUT	14.37	121.02	6.26	192.22	1.03	1564	1841	1989
Guam	GAM	13.58	144.87	5.61	215.55	1.03	1554	1840	1986
Biak	BIK	−1.08	136.05	−9.73	207.39	1.05	1546	1823	1985

the Pi2 onset of this event. The selected models for each interval are $m^*_{:\xi^*_{-1}} = 1$ and $m^*_{\xi^*:N} = 2$.

[28] We applied the procedure to data from other stations of the 210°. MM Observation Network. The coordinates of those stations are listed in Table 1 [*Yumoto et al.*, 1996]. We used the same data windows and search intervals. Figure 10a shows the first wave packet. Here the data are detrended and are normalized by their range over the interval of the plot. The vertical bar marks the estimated onset time, and its length corresponds to 0.5 nT for each station. Figures 10b and 10c show the results for the second and the third wave packets, respectively, in the same format used in Figure 10a.

6. Discussion

[29] The onset times determined by our procedure for the second and third wave packets at KAK are $\xi^*_{[1]}$ = 1330:35 (1835 s) and $\xi^*_{[2]}$ = 1333:05 (1985 s), respectively, which are 15 s later than the onset times that *Kepko and McPherron* [2001] determined by the 1/3 maximum amplitude method. Whereas *Kepko and McPherron* [2001] determined the onset of each packet by combining data from seven stations of the same network, our procedure determines an onset for each station. We did not show the result for the BSV data because of a possible timing problem of the data for this event.

[30] *Kepko and McPherron* [2001] defined the Pi2 onset as a time when the wave amplitude of a filtered component reaches a certain fraction of the maximum phase amplitude of the wave packet (1/3 in the first approach of *Kepko and McPherron* [2001]). *Tsunezawa et al.* [1999] used a "filtered" signal (running average of 20 s) and evaluated the peaks of the oscillation. The method adopted by *Takahashi et al.* [1995] also focuses on the envelope function of the wave amplitude. Any method based on a wavelet analysis examines the wavelet coefficients for some ranges in frequency domain [*Nose' et al.*, 1998], and thus it can also be regarded as based on the same concept.

[31] We emphasize that analyzing lower-frequency components is essentially the same as analyzing smoothed (filtered) data. If the background magnetic field and/or the amplitude of noisy components change around the initial period of Pi2 pulsations, any linear band-pass filter generates a pseudo precursor prior to a true onset time, making an estimated onset earlier than the real one. Therefore we must avoid an artifact of applying the band-pass filter. In addition, the threshold for selecting the Pi2 pulsation such as 1/3 and a factor of 10 is arbitrary, which also reduces the precision of the estimated onset time. In contrast, our procedure does not filter or smooth data, rather it analyzes the original data. It determines the Pi2 onset so that intervals before and after the onset can be optimally described by different models. The onset determined therefore has the same precision as the sampling time of the data.

[32] *Uozumi et al.* [2000] examined the latitudinal dependence of the time when the energy fluctuation reaches its maximum. Whereas their studies examined the (apparent) spatial propagation of Pi2 waves based on the timing of the peak amplitude or the phase of oscillation, our procedure allows us to discuss the very initial signature of Pi2 waves. Thus the result should be more informative on the excitation mechanism of Pi2 waves. For the first wave packet we can see the tendency for the onset time to become later as approaching the magnetic equator, especially if we disregard MGD, the result for which is likely to be affected by the less qualified data. In contrast, the tendency is not very clear for the second package. Obviously, a more extensive study is necessary for addressing the latitudinal dependence of the onset time, which, however, is beyond the scope of the present paper.

[33] As demonstrated in Figure 5, our procedure enables us to identify an optimal ξ, ξ^*, by which two different wave packets are separated in time domain. For the third wave packet in the actual application, ξ^* appears to be determined around a point where we may observe a phase skip: as typically demonstrated in Figure 9, the third wave packet starts with a positive phase during an interval for which the second wave packet obviously takes a positive phase. Figure 10c clearly shows that this tendency is common to all stations. It has been reported that the Pi2 pulsations observed at high-latitude and midlatitude ground stations on the nightside often exhibit phase skips [*Meir-Jedrzejowicz and Hughes*, 1980; *Kepko and Kivelson*, 1999]. A dependency of ξ^* on the locations of the stations, i.e., latitudinal dependency, seems to be insignificant in comparison with those for the first and second wave packets: the ranges of ξ^* for the first, second, and third wave packets are 19, 18, and 5 s, respectively. No clear geophysical interpretation can be given to this insignificant difference for the third wave packet: we need more case studies that involve two different wave packets observed successively.

[34] In the actual data analysis (section 5), we imposed conditions relating to the sign of phase in the first half wave cycle because it is believed that a Pi2 pulsation at low-latitudes and midlatitudes starts with a positive phase as a result of phenomena associated with a compressional wave process. Actually, the Cauchy wavelet which starts with a positive deviation is adopted as the mother wavelet in an analysis of the Pi2 pulsation because its shape is similar to that of Pi2 pulsation [*Tsunezawa et al.*, 1999]. Other mother wavelets used in the wavelet analysis for the Pi2 pulsation, the Mayer wavelet and the Gabor wavelet, are apart from this characteristics [*Nose' et al.*, 1998; *Tsunezawa et al.*, 1999].

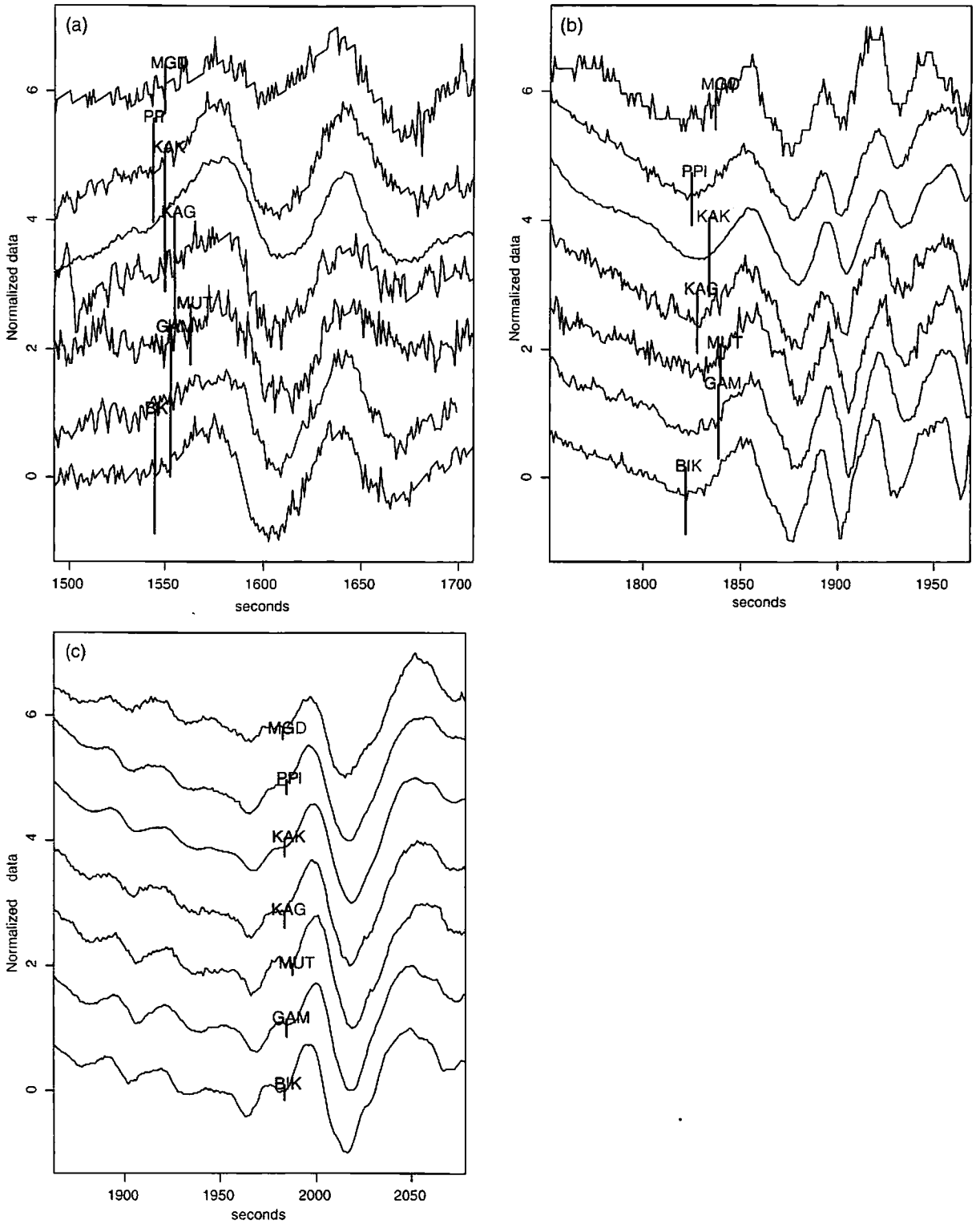

Figure 10. (a) Normalized data for the first wave packet. The location and length of the vertical bars indicate the estimated onset time and unit of 0.5 nT for each station. (b) Normalized data for the second wave packet. (c) Normalized data for the third wave packet.

and then unfavorable in terms of the sensitivity to detect an initial deviation of the Pi2 pulsation. This condition on the sign of phase allows us to exclude ξ from a candidate for an optimal ξ, when AIC(ξ) attains the minimum value at ξ, but the decomposed QPO component starts with a negative phase. Then the small fluctuation of the trend component around a true onset time is no longer diagnosed as the QPO component insofar as the small fluctuation starts with

negative phase. In other words, imposing this condition makes an estimate of the onset time robust against the small fluctuation of the trend component. Consequently, if coherent wave patterns are observed at several stations, imposing this condition helps our procedure identify these wave patterns as the QPO component and then makes physically reasonable a wave propagation speed estimation based on an analysis of the onset times at multiple stations. Meanwhile, it is shown in the simulation data analysis (section 4) that our procedure without this condition is capable of detecting an onset time of the Pi2 pulsation irrespective of the sign of initial phase. Then if a concept related to initial phase is subject to questionable, our procedure provides us with a diagnosis to examine this concept.

7. Summary

[35] The advantages of applying our procedure are summarized as two points. First our model for onset time determination is conceptually based on the approach of switching the time series model at an onset time, and then it is free from an artificial signature, which is inherent to any linear band-pass filter. Second the onset time, which is defined as an optimal partition of the time series, can be objectively determined by minimizing the Akaike information criterion. Our method is free from the ambiguity of onset time determination. Accordingly, our procedure enables us to determine an onset time of Pi2 pulsations with a precision of the sampling time of data. Excellent performance in estimating the onset time precisely was illustrated by applying our procedure to simulation and actual data sets in each of which a typical Pi2 pulsation is observed.

Appendix: Kalman Filter and Smoother

[36] Here we briefly explain the Kalman filter along with the model for $H_{\xi:N}$. More detailed explanation is given by *Kitagawa* [1981], *Higuchi* [1991], and *Kitagawa and Gersch* [1996].

[37] The first step of the recursive calculation of the state vector is to give a proper initial distribution, $p(\mathbf{x}_{\xi-1}^{(m)}|\phi)$, which is assumed to be a Gaussian distribution with an initial mean vector $\mathbf{x}_{\xi-1|\xi-1}^{(m)}$ and variance matrix $V_{\xi-1|\xi-1}^{(m)}$. Here ϕ is a parameter vector for specifying $\mathbf{x}_{\xi-1|\xi-1}^{(m)}$ and $V_{\xi-1|\xi-1}^{(m)}$. Usually $\mathbf{x}_{\xi-1|\xi-1}^{(m)}$ and $V_{\xi-1|\xi-1}^{(m)}$ are given by a zero vector and a diagonal matrix diag $(c, \ldots, c)$, where c is a large value (for example $c = 10^6$). Of course, proper treatment to include prior information on a distribution of $\mathbf{x}_{\xi-1}^{(m)}$ is recommended in practice. For example, we can employ state variable values of $\mathbf{x}_{\xi-1|\xi-1}^{(m')}$, where $\mathbf{x}_{\xi-1|\xi-1}^{(m')}$ is a final estimate of $\mathbf{x}_{\xi-1}^{(m')}$ given $H_{1:\xi-1}$ and m' denotes the time series model adopted for $H_{1:\xi-1}$.

[38] The procedure repeats the following prediction and filter alternately from $n = \xi$ through $n = N$ and saves a set of $Z^{(m)} = \{(\mathbf{x}_{n|n-1}^{(m)}, V_{n|n-1}^{(m)}, \mathbf{x}_{n|n}^{(m)}, V_{n|n}^{(m)}) \mid n = \xi, \ldots, N\}$.

Prediction

$$\mathbf{x}_{n|n-1}^{(m)} = F^{(m)}\mathbf{x}_{n-1|n-1}^{(m)}$$
$$V_{n|n-1}^{(m)} = F^{(m)}V_{n-1|n-1}^{(m)}F^{(m)'} + G^{(m)}R^{(m)}G^{(m)'} \quad \text{(A1)}$$

Filtering

$$\mathbf{x}_{n|n}^{(m)} = \mathbf{x}_{n|n-1}^{(m)} + e_n^{(m)}K_n^{(m)}$$
$$V_{n|n}^{(m)} = V_{n|n-1}^{(m)} - K_n^{(m)}D^{(m)}V_{n|n-1}^{(m)}. \quad \text{(A2)}$$

where

$$u_n^{(m)} = D^{(m)}V_{n|n-1}^{(m)}D^{(m)'} + 1$$
$$K_n^{(m)} = \frac{1}{u_n^{(m)}}V_{n|n-1}^{(m)}D^{(m)'}$$
$$e_n^{(m)} = H_n - D^{(m)}\mathbf{x}_{n|n-1}^{(m)}.$$

[39] The likelihood of H_n, $p(H_n|H_{\xi:n-1}, \theta^{(m)})$, is defined as a by-product in this filtering step.

$$p\left(H_n|H_{\xi:n-1}, \theta^{(m)}\right) = \frac{1}{\sqrt{2\pi\sigma^{2,(m)}u_n^{(m)}}}\exp\left(-\frac{\left(e_n^{(m)}\right)^2}{2\sigma^{2,(m)}u_n^{(m)}}\right). \quad \text{(A3)}$$

[40] The $\partial\ell(H_{\xi:N}|\theta^{(m)})/\partial\sigma^{2,(m)}$ yields an estimate of the variance of the observation noise

$$\hat{\sigma}^{2,(m)} = \frac{1}{N-\xi+1}\sum_{n=\xi}^{N}\frac{\left(e_n^{(m)}\right)^2}{u_n^{(m)}}. \quad \text{(A4)}$$

Then the maximization of $\ell(H_{\xi:N}|\theta^{(m)})$ with respect to $\theta^{(m)}$ can be simplified to a nonlinear maximization problem under the assumption that $\sigma^{2,(m)} = \hat{\sigma}^{2,(m)}$.

[41] The smoothing algorithm estimates the state vector at any time of n, $\mathbf{x}_n^{(m)}$, based on all data points, i.e., $H_{\xi:N}$. It should be remembered that the estimate of the state vector $\mathbf{x}_n^{(m)}$ with the Kalman filter algorithm is based on the observations from ξ up to n, i.e., $H_{\xi:n}$. The efficient calculation of estimating $\mathbf{x}_{n:N}^{(m)}$ is achieved by using a set $Z^{(m)}$ which has already been determined by applying the Kalman filter. Repeat the following step backward in time, i.e., from $n = N$ through $n = \xi$.

Smoothing

$$\mathbf{x}_{n|N}^{(m)} = \mathbf{x}_{n|n}^{(m)} + -A_n^{(m)}\left(\mathbf{x}_{n+1|N}^{(m)} - \mathbf{x}_{n+1|n}^{(m)}\right)$$
$$V_{n|N}^{(m)} = V_{n|n}^{(m)} + A_n^{(m)}\left(V_{n+1|N}^{(m)} - V_{n+1|n}^{(m)}\right)A_n^{(m)'}, \quad \text{(A5)}$$

where

$$A_n^{(m)} = V_{n|n}^{(m)}F^{(m)'}V_{n+1|n}^{(m)-1}.$$

Define an estimate of the state vector for given $\theta^{(m)}$, $\hat{\mathbf{x}}_n^{(m)}$, by $\hat{\mathbf{x}}_n^{(m)} = \mathbf{x}_{n|N}^{(m)}$.

[42] Acknowledgments. Work at the Institute of Statistical Mathematics was carried out in part under the ISM cooperative Research Program (H11-2040 and H12-2026) and Grant-in-Aid for Scientific Research (B) (12558023). We would like to thank Dr. Nose' and Dr. Takahashi at JHU/APL for useful discussions.

[43] Janet G. Luhmann thanks Peter R. Sutcliffe and another referee for their assistance in evaluating this paper.

References

Akaike, H., A new look at the statistical model identification, *IEEE Trans. Autom. Control, AC-19*, 716, 1974.

Akaike, H., and G. Kitagawa (Eds.), *The Practice of Time Series Analysis*, Springer-Verlag, New York, 1998.

Anderson, B. D. O., and J. B. Moore, *Optional Filtering*, Prentice-Hall, Englewood Cliff, N. J., 1979.

CPMN Group, Characteristics of pi2 magnetic pulsations observed at the CPMN stations: A review of STEP results, *Earth Planet Space, 53*, 981, 2001.

Higuchi, T., Method to subtract an effect of the geocorona EUV radiation from the low energy particle (LEP) data by the Akebono (EXOS-D) satellite, *J. Geomag. Geoelectr., 43*, 957, 1991.

Higuchi, T., K. Kita, and T. Ogawa, Bayesian statistical inference to remove periodic noises in the optical observation aboard a spacecraft, *Appl. Opt., 27*, 4514, 1988.

Itonaga, M., and T.-I. Kitamura, Smoothing of geomagnetic data using a piecewise cubic polynomial, *Geophys. J. Int., 116*, 655, 1994.

Kitagawa, G., A nonstationary time series model and its fitting by a recursive filter, *J. Time Ser. Anal., 2*, 103, 1981.

Kitagawa, G., and W. Gersch, *Smoothness Priors Analysis of Time Series*, Springer-Verlag, New York, 1996.

Kepko, L., and M. Kivelson, Generation of Pi2 pulsations by bursty bulk flow, *J. Geophys. Res., 104*, 25,021, 1999.

Kepko, L., and R. L. McPherron, Comment on "Evaluation of low-latitude Pi2 pulsations as indicators of substorm onset using Polar ultraviolet imagery" by K. Liou et al., *J. Geophys. Res., 106*, 18,919, 2001.

Liou, K., C.-I. Meng, P. T. Newell, K. Takahashi, S.-I. Ohtani, A. T. Y. Lui, M. Brittnacher, and G. Parks, Evaluation of low-latitude Pi2 pulsations as indicators of substorm onset using Polar ultraviolet imagery, *J. Geophys. Res., 105*, 2495, 2000.

Liou, K., P. T. Newell, C.-I. Meng, K. Takahashi, S. Ohtani, A. T. Y. Lui, M. Brittnacher, and G. Parks, Reply, *J. Geophys. Res., 106*, 18,923, 2001.

Meir-Jedrzejowicz, W. A. C., and W. J. Hughes, Phase skipping and packet structure in geomagnetic pulsation signals, *J. Geophys. Res., 85*, 6888, 1980.

Nagai, T., M. Fujimoto, Y. Saito, S. Machida, T. Terasawa, R. Nakamura, T. Yamamoto, T. Mukai, A. Nishida, and S. Kokubun, Structure and dynamics of magnetic reconnection for substorm onsets with Geotail observations, *J. Geophys. Res., 103*, 4419, 1998.

Nose', M., T. Iyemori, and M. Takeda, Automated detection of Pi2 pulsations using wavelet analysis, 1, Method and application for substorm monitoring, *Earth Planets Space, 50*, 773, 1998.

Ohtani, S., K. Takahashi, T. Higuchi, A. T. Y. Lui, and H. E. Spence, AMPTE/CCE-SCATHA simultaneous observations of substorm-associated magnetic fluctuations, *J. Geophys. Res., 103*, 4671, 1998.

Ohtani, S., F. Creutzberg, T. Mukai, H. Singer, A. T. Y. Lui, M. Nakamura, P. Prikryl, K. Yumoto, and G. Rostoker, Substorm onset timing: The December 31, 1995, event, *J. Geophys. Res., 104*, 22,713, 1999.

Olson, J. V., Pi2 pulsations and substorm onsets: A review, *J. Geophys. Res., 104*, 17,499, 1999.

Saito, T., K. Yumoto, and Y. Koyama, Magnetic pulsation Pi2 as a sensitive indicator of magnetospheric substorm, *Planet. Space Sci., 24*, 1025, 1976.

Sakamoto, Y., M. Ishiguro, and G. Kitagawa, *Akaike Information Criterion statistics: Mathematics and its application*, D. Reidel, Norwell, Mass., 1986.

Sergeev, V. A., V. Angelopoulos, D. G. Mitchell, and C. T. Russell, In situ observations magnetotail reconnection prior to the onset of a small substorm, *J. Geophys. Res., 100*, 19,121, 1995.

Shiokawa, K., et al., High-speed ion flow, substorm current wedge, and multiple Pi 2 pulsations, *J. Geophys. Res., 103*, 4491, 1998.

Sutcliffe, P. R., Substorm onset identification using neural networks and Pi2 pulsations, *Ann. Geophys., 15*, 1257, 1997.

Takahashi, K., S. Ohtani, and B. J. Anderson, Statistical analysis of Pi2 pulsations observed by the AMPTE CCE spacecraft in the inner magnetosphere, *J. Geophys. Res., 100*, 21,929, 1995.

Takanami, T., High precision estimation of seismic wave arrival times, in *The Practice of Time Series Analysis*, edited by H. Akaike and G. Kitagawa, p. 79, Springer-Verlag, New York, 1998.

Tsunezawa, K., Y. Tonegawa, and T. Sakurai, Detection of the onset time of Pi2 pulsations by using wavelet analysis, *Adv. Polar Upper Atmos. Res., 13*, 154, 1999.

Uozumi, T., K. Yumoto, H. Kawano, A. Yoshikawa, J. V. Olson, S. L. Solovyev, and E. F. Vershinin, Characteristics of energy transfer of Pi2 magnetic pulsations: Latitudinal dependence, *Geophys. Res. Lett., 27*, 1619, 2000.

Yumoto, K., and the 210° MM Magnetic Observation Group, The STEP 210° magnetic meridian network project, *J. Geomag. Geoelectr., 48*, 1297, 1996.

T. Higuchi, The Institute of Statistical Mathematics, Tokyo 106-8569, Japan. (higuchi@ism.ac.jp)

S. Ohtani, The Johns Hopkins University Applied Physics Laboratory, Johns Hopkins Road, Laurel, MD 20723-6099, USA. (ohtani@jhuapl.edu)

T. Uozumi and K. Yumoto, Department of Earth and Planetary Sciences, Kyushu University, 6-10-1 Hakozaki Fukuoka, 812-0053, Japan. (uozumi@geo.kyushu-u.ac.jp; yumoto@geo.kyushu-u.ac.jp)